mathematics

MDPI

Article

A Scheme for Generating Millimeter Wave Signals through 32-Tupling Frequency Multiplication without Filtering Using Eight Mach-Zehnder Modulators

Xiangqing Wang [1,2,3,4,5,*], Lei Ren [2], Xiaokun Yang [1,3,4] and Dongfei Wang [1,3]

[1] School of Electronic Information, Nanchang Institute of Technology, Nanchang 330099, China; yangxk@bupt.cn (X.Y.); wdfchina@bigc.edu.cn (D.W.)
[2] School of Physics and Electronic Engineering, Fuyang Normal University, Fuyang 236037, China; 22221125@fynu.edu.cn
[3] School of Artificial Intelligence, Wuhan Technology and Business University, Wuhan 430065, China
[4] Advanced Cryptography and System Security Key Laboratory of Sichuan Province, Chengdu 610054, China
[5] Henan Key Laboratory of Visible Light Communications, Zhengzhou 450001, China
* Correspondence: wxqing@fynu.edu.cn

Abstract: In this paper, a filterless 32-tupling millimeter wave generation scheme based on eight MZMs is proposed. The system has an upper and lower parallel two-branch structure. The upper branch consists of two subsystems Sub-A and Sub-B in cascade, each subsystem contains four MZMs, and the MZMs are all operating at maximum transfer point (MATP). Sub-A mainly generates ±8th order optical sideband signal as the incident light signal of Sub-B. After modulation of Sub−B, the output signal is mainly ±16th order optical sideband signal containing the central optical carrier component. The optical attenuator (OATT) and optical phase shifter (OPS) of the lower branch are used to regulate the phase and amplitude of the optical carrier. The upper and lower branches are coupled, and the central optical carrier component is superimposed and cancelled so only the ±16th order optical sideband signal is retained. Finally, the 32-tupling frequency millimeter is generated by the photodiode (PD) receiver after photoelectric detection which receives and generates a 32-tupling frequency millimeter wave signal. The simulation results show that the 160 GHz millimeter wave signal can be obtained by driving the MZM with a 5 GHz RF signal, and the optical sideband suppression ratio (OSSR) and the RF sideband suppression ratio (RFSSR) are 52.6 dB and 44.75 dB, respectively. Theoretical analysis and simulation experiments are carried out for the proposed scheme which proves the feasibility of the scheme.

Keywords: external modulation; frequency 32-tupling; Mach-Zehnder Modulator (MZM); anxiety-free wave

MSC: 78M99

Citation: Wang, X.; Ren, L.; Yang, X.; Wang, D. A Scheme for Generating Millimeter Wave Signals through 32-Tupling Frequency Multiplication without Filtering Using Eight Mach-Zehnder Modulators. *Mathematics* **2024**, *12*, 2781. https://doi.org/10.3390/math12172781

Academic Editor: Jonathan Blackledge

Received: 11 June 2024
Revised: 1 September 2024
Accepted: 3 September 2024
Published: 8 September 2024

1. Introduction

With the rapid development of mobile communication technologies, the standardization of 5G has been completed and commercial deployments have been completed in several cities around the world. However, due to the increasing number of connected devices and users and the exponential rise in data traffic, the number of device connections per cubic meter will be in the hundreds. In addition, the continuous emergence of various applications and scenarios, such as automated driving, virtual reality, 4 K/8 K UHD video, 3D communication, digital twins, and other applications and scenarios not yet foreseen [1,2], mean it will be difficult for the currently deployed 5G communications to meet the data rate and ultra-low latency requirements of these applications. These challenges are considered key drivers for the development of next generation mobile communication systems. Millimeter wave (MM wave) refers to electromagnetic waves with wavelengths

at the millimeter level, usually in the frequency band from 30 GHz to 300 GHz. Terahertz waves, which refer to electromagnetic waves with frequencies in the range of 0.1–10 THz (wavelengths of 3000–30 μm), overlap with millimeter waves in the long wavelength band and with infrared light in the short wavelength band [3,4]. Due to their high frequency and short wavelength characteristics, millimeter/terahertz waves have strong penetration, high resolution, and sensitivity to interaction with matter, making them promising for a wide range of applications in several fields, such as fibre-optic radio systems [5] and radar [6]. The increase in user demand for broadband and the shortage of available spectrum resources have moved the carrier frequency of wireless communications to the millimeter and terahertz bands [7–9]. However, since the conventional millimeter/terahertz wave generation in the electric domain is limited by bottlenecks in electronic devices, it is difficult to generate millimeter wave signals at frequencies exceeding 100 GHz [10]. Therefore, the current technology for millimeter/terahertz wave generation research has shifted to the optical domain. Generating millimeter/terahertz waves in the optical domain can effectively overcome the limitations imposed by electronic bottlenecks and greatly improve the complexity and cost of millimeter/terahertz wave generation systems [11]. The method of generating millimeter/terahertz waves in the optical domain has become a popular research topic in recent years.

Currently, the techniques used to generate millimeter waves cover optical aberration [12], frequency upconversion [13], four-wave frequency mixing [14,15], stimulated Brillouin scattering [16,17], direct modulation [18], and external modulation techniques [19]. Despite the simplicity and ease of use of optical aberration and frequency upconversion, they suffer from phase noise and signal frequency limitation, while four-wave mixing and stimulated Brillouin scattering can generate millimeter waves, but the systems are complex and have limited multiplication factors. In contrast, the external modulation technique, with its high reliability, large multiplication factor and good frequency tunability, is a more reliable and flexible scheme for millimeter wave generation. In the literature [20], the method of using wavelength-selective switching cascade external modulator can generate four-octave or six-octave frequency, but the system structure is complicated. In the literature [21], 12-tupling frequency without an optical filter was achieved using two parallel MZMs. In the literature [22], a millimeter wave generation scheme that eliminates the central optical carrier component by using the OPS cascade OATT coupling was proposed based on two parallel MZMs to achieve 16-tupling frequency without optical filter, which further improves the multiplication factor of the system, but the spectral purity of the generated signals was not high. In the literature [23], a large number of passive optical components were used in the proposed scheme, which increased the insertion loss of the system and reduced the stability and reliability of the system, and in the literature [24], a 16-tupling frequency millimeter wave filterless generation scheme based on four MZMs was proposed to generate only $\pm$8th order optical sidebands by appropriately adjusting the bias parameter of the MZMs and the phase of the RF signals, and in the literature [25], an optical sideband of only $\pm$8th order was generated by utilizing eight MZMs in parallel structure to achieve a 32-tupling frequency of the signal. The generated millimeter wave signal had a high sideband rejection ratio, but the modulation index in this scheme was as high as 18.07, which is not easy to achieve. To address the above problems, this paper proposes a novel 32-tupling millimeter wave generation scheme which can ensure that the generated millimeter wave signals have a high OSSR and RFSSR at the same time and can further reduce the power consumption of the system, as well as reduce the system requirements for the modulation index. Reducing the electrical stress caused by the high driving voltage of the MZM extends the service life of the equipment and improves the overall reliability and stability of the system.

2. Operational Principle

Figure 1 shows the schematic structure of the 32-tupling millimeter wave generation system, with figures (a), (b), (c), and (d) displaying the optical sideband outputs at each

point of the system. The system consists of a continuous laser wave transmitter, 8 MZM modulators, OPS, electrical phase shifter (EPS), optical amplifier (OA), OATT, and other devices. The MZM is used to modulate the input optical signal, and its basic structure usually includes an input optical waveguide, a 3 dB power splitter, and a coupler [26]. A 3 dB power splitter divides light into two branches (or upper and lower arms) in a Y-branch structure, with electrodes on both branches used to apply voltage to change the phase of the light, and a Y-branch structure with a coupler used to recombine the light from the two branches. When the voltages loaded onto the upper and lower arms of MZM are $u_1(t)$ and $u_2(t)$, respectively, intensity modulation or phase modulation can be achieved by reasonably controlling the driving voltage of the upper and lower arms. The OPS and EPS are used to adjust the phase of the input optical signal and RF driving signal respectively, the OA is used to compensate for the loss of the optical signal during the modulation process, and the lower optical branch cascaded with the OATT and OPS is used to cancel out the stray central optical sideband component generated during the modulation process [22].

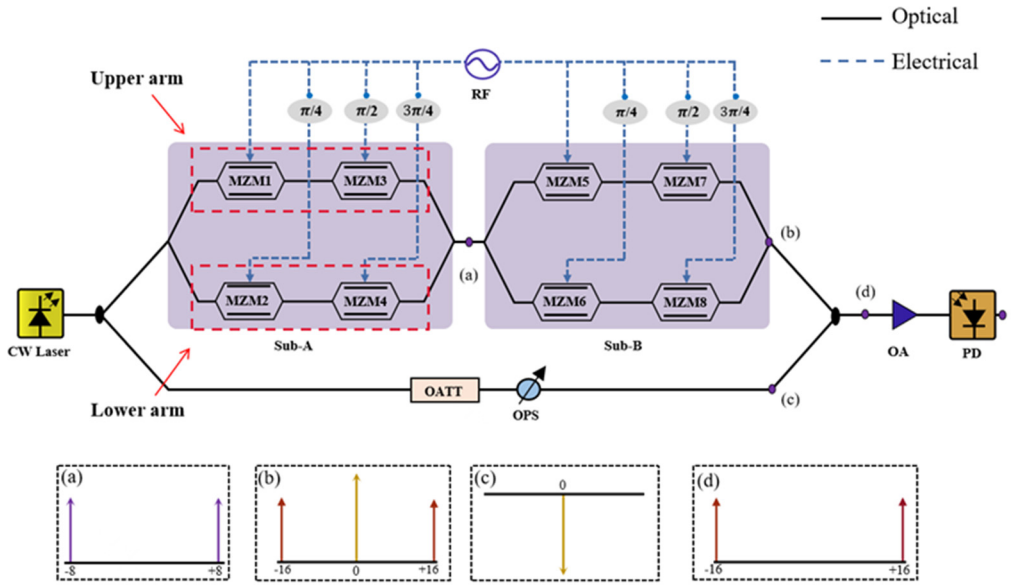

Figure 1. 32nd harmonic millimeter wave generation system structure: (**a**) spectrum of signal modulated by Sub-A; (**b**) spectrum of signal modulated by Sub-B; (**c**) the optical carrier of the signal after OATT and OPS; (**d**) spectral analysis of the coupled output signal.

In the proposed 32-tupling millimeter wave generation system, the output optical signal is divided into upper and lower branches, with the upper branch consisting of two cascaded Sub-A and Sub-B subsystems. All MZMs work on MATP to output only even order optical sideband signals. By setting the initial RF drive signal phases of MZM1, MZM2, MZM3, and MZM4 to 0, 45°, 90°, and 135°, respectively, the modulation output of Sub-A only contains ±8th order optical sideband signals. In Sub-B, the optical signal output by Sub-A is used as the incident optical signal again. After modulation and output by Sub-B, it is coupled with the optical carrier signal component output by the lower optical splitter to maximize the amplitude of the ±16th order optical sideband in the output optical signal component. After amplification by the OA, it is received by the PD to generate a 32-tupling millimeter wave.

3. Theoretical Analysis

Assuming that the optical carrier signal output from the continuous wave laser is $E_{in} = E_c \exp(\mathrm{j}\omega_c t)$, where E_c and ω_c are the amplitude and frequency of the optical carrier signal, and the RF signal is $V = V_m \cos(\omega_{R_f} t)$, where V_m and ω_{R_f} are the amplitude and frequency of the RF drive signal, if the drive voltages loaded to the upper and lower arms

of the MZM are V_1 and V_2, respectively, then for a single MZM, when the MZM is operating at the maximum transmission point, i.e., when there is a phase difference of π between the upper and lower arms of the MZM [27], the output can be expressed as

$$\begin{aligned} E_{out} &= \alpha E_{in}[\gamma \exp(j\varphi_1) + (1 - \gamma)\exp(j\varphi_2)] \\ &= E_{in}\left[\gamma \exp\left(j\pi \frac{V_{DC2}+V_2}{V_\pi}\right)\right. \\ &\left.+(1 - \gamma)\exp\left(j\pi \frac{V_{DC1}+V_1}{V_\pi}\right)\right] \end{aligned} \tag{1}$$

Assuming that γ = 0.5 in the ideal operating state of MZM, when MZM operates in MATP, there is no DC bias when the input optical signal is $E_{in} = E_0 e^{j\omega_0 t}$. According to the above equation the output of MZM [28] can be further expressed as

$$\begin{aligned} E_{MZM} &= \alpha E_{in}[\exp(j\varphi_1) + \exp(j\varphi_2)] \\ &= \alpha E_{in}\left[\exp\left(j\pi \frac{V_m \cos(\omega_{R_f} t+\theta_1)}{V_\pi}\right) + \exp\left(j\pi \frac{V_m \cos(\omega_{R_f} t+\theta_1+\pi)}{V_\pi}\right)\right] \\ &= 2\alpha E_{in} \sum_{n=-\infty}^{\infty} (-1)^n J_{2n}(m) e^{j2n\omega_{R_f} t} \end{aligned} \tag{2}$$

where φ_1 and φ_2 are denoted as the phase changes of the upper and lower arms of the MZM caused by the RF drive signals loaded onto the MZM with the DC bias, respectively, and $V_m \cos(\omega_{R_f} t + \theta_1)$ and $V_m \cos(\omega_{R_f} t + \theta_1 + \pi)$ are the RF drive signals loaded onto the upper and lower arms of the MZM, respectively.

In Sub-A, when the initial phase $\theta_i (i = 1, 2, 3, 4)$ of the drive signal loaded onto the MZM is set to be 0, $\pi/4$, $\pi/2$, $3\pi/4$, respectively, according to Equation (2) the outputs of the MZM1–MZM4 can be expressed as

$$\begin{aligned} E_{MZM1} &= \alpha E_{in} \sum_{n=-\infty}^{\infty} j^n J_n(m) e^{jn\omega_{R_f} t}\left[1 + e^{jn\pi}\right] \\ &= 2\alpha E_{in} \sum_{n=-\infty}^{\infty} (-1)^n J_{2n}(m) e^{j2n\omega_{R_f} t} \end{aligned} \tag{3}$$

$$\begin{aligned} E_{MZM2} &= \alpha E_{in} \sum_{n=-\infty}^{\infty} j^n J_n(m) e^{jn\omega_{R_f} t} e^{jn\frac{\pi}{4}}\left[1 + e^{jn\pi}\right] \\ &= 2\alpha E_{in} \sum_{n=-\infty}^{\infty} (-1)^n J_{2n}(m) e^{j2n(\omega_{R_f} t+\frac{\pi}{4})} \end{aligned} \tag{4}$$

$$\begin{aligned} E_{MZM3} &= \alpha E_{in} \sum_{n=-\infty}^{\infty} j^n J_n(m) e^{jn\omega_{R_f} t} e^{jn\frac{\pi}{2}}\left[1 + e^{jn\pi}\right] \\ &= 2\alpha E_{in} \sum_{n=-\infty}^{\infty} (-1)^n J_{2n}(m) e^{j2n(\omega_{R_f} t+\frac{\pi}{2})} \end{aligned} \tag{5}$$

$$\begin{aligned} E_{MZM4} &= \alpha E_{in} \sum_{n=-\infty}^{\infty} j^n J_n(m) e^{jn\omega_{R_f} t} e^{jn\frac{3\pi}{4}}\left[1 + e^{jn\pi}\right] \\ &= 2\alpha E_{in} \sum_{n=-\infty}^{\infty} (-1)^n J_{2n}(m) e^{j2n(\omega_{R_f} t+\frac{3\pi}{4})} \end{aligned} \tag{6}$$

Through Equations (3)–(6), it can be seen that the odd-order optical sidebands are suppressed in the outputs of MZM1–MZM4, and the outputs only contain ±2nd order optical sideband signals.

In the subsystem Sub-A composed of MZM1-MZM4, the upper arm and lower arm of the subsystem are composed of MZM1 and MZM3 and MZM2 and MZM4 in cascade, respectively, and thus according to Equations (3) and (5), the output of the upper arm in Sub-A can be expressed as

$$\begin{aligned} E_U &= E_{MZM1} \times E_{MZM3} \\ &= 2\alpha E_{MZM1} \sum_{n=-\infty}^{\infty} (-1)^n J_{2n}(m) e^{j2n(\omega_{R_f} t + \frac{\pi}{2})} \\ &= 4\alpha^2 E_{in} \Big\{ \Big[J_0(m)^2 - 2J_2(m)^2 + 2J_4(m)^2 - 2J_6(m)^2 \Big] - 2\Big[J_2(m)^2 \cos\Big(4\omega_{R_f} t\Big) \\ &\quad - J_4(m)^2 \cos\Big(8\omega_{R_f} t\Big) + J_6(m)^2 \Big(12\omega_{R_f} t\Big) - 2J_0 J_4 \cos\Big(4\omega_{R_f} t\Big) + 2J_2 J_6 \cos\Big(4\omega_{R_f} t\Big) + 2J_2 J_6 \cos\Big(8\omega_{R_f} t\Big) \Big] \Big\} \end{aligned} \tag{7}$$

According to Equations (4) and (6) the output of lower arm can be expressed as

$$\begin{aligned} E_L &= E_{MZM2} \times E_{MZM4} \\ &= 2\alpha E_{MZM2} \sum_{n=-\infty}^{\infty} (-1)^n J_{2n}(m) e^{j2n(\omega_{R_f} t + \frac{3\pi}{4})} \\ &= 4\alpha^2 E_{in} \Big\{ \Big[J_0(m)^2 - 2J_2(m)^2 + 2J_4(m)^2 - 2J_6(m)^2 \Big] + 2\Big[J_2(m)^2 \cos\Big(4\omega_{R_f} t\Big) \\ &\quad + J_4(m)^2 \cos\Big(8\omega_{R_f} t\Big) + J_6(m)^2 \cos\Big(12\omega_{R_f} t\Big) - 2J_2(m) J_6(m) \cos\Big(8\omega_{R_f} t\Big) \\ &\quad - 2J_0(m) J_4(m) \cos\Big(4\omega_{R_f} t\Big) + 2J_2(m) J_6(m) \cos\Big(4\omega_{R_f} t\Big) \Big] \Big\} \end{aligned} \tag{8}$$

From Equations (7) and (8), it can be seen that the optical sideband signal components in the outputs of the upper arm and the lower arm in Sub-A both contain the 0th order optical carrier signal, ±4th, ±8th, and ±12th order optical sideband signals, but due to a 45° phase difference in the initial phase of the RF drive signal between the upper and lower arms, the ±4th and ±12th order optical sideband components in the optical signal components output by the upper and lower arms are a group of optical signal components with the same amplitude and opposite phase. Therefore, when the optical signals output by the upper and lower arms of the system are coupled and output through an optical coupler, the stray ±4th and ±12th order optical sideband components will be cancelled out. At this time, the output of Sub-A can be expressed as

$$\begin{aligned} E_{Sub-A} &= E_U + E_L \\ &= 8\alpha^2 E_{in} \Big\{ \Big[J_0(m)^2 - 2J_2(m)^2 + 2J_4(m)^2 - 2J_6(m)^2 \Big] \\ &\quad + 2\Big[J_4(m)^2 - 2J_2(m) J_6(m) \Big] \cos\Big(8\omega_{R_f} t\Big) \Big\} \end{aligned} \tag{9}$$

In Figure 2, Cn is the term coefficient of $\cos\Big(8n\omega_{R_f} t\Big)$ (n = 0, 1, 2), so that $C_0 = J_0(m)^2 - 2J_2(m)^2 + 2J_4(m)^2 - 2J_6(m)^2$. C8 and C16 are the optical sideband signals to be retained and, according to Figure 2, it can be seen that when the modulation index is set to be m = 6.12, $C_0 \approx 0$, which can be ignored, and at this time, Equation (9) can be further simplified as

$$\begin{aligned} E_{Sub-A} &= E_U + E_L \\ &= 8\alpha^2 E_{in} \Big\{ \Big[J_4(m)^2 - 2J_2(m) J_6(m) \Big] \cos\Big(8\omega_{R_f} t\Big) \Big\} \\ &= 8\alpha^2 E_{in} \Big\{ C_8 \cos\Big(8\omega_{R_f} t\Big) \Big\} \end{aligned} \tag{10}$$

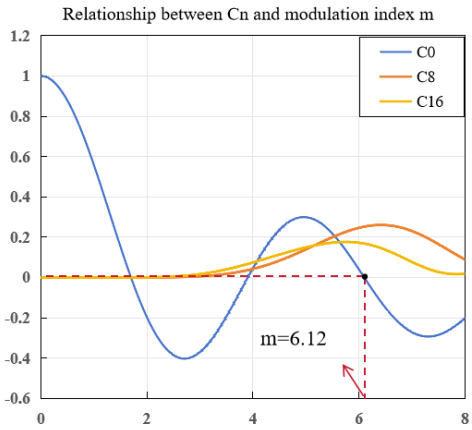

Figure 2. The relationship between Cn and modulation index m.

Since Sub-A and Sub-B are cascaded and have similar structures, at this time, for Sub-B, the output optical signal of Sub-A is the incident optical signal of Sub-B, so the output of Sub-B can be expressed as

$$\begin{aligned} E_{Sub-B} &= E_{Sub-A} \times E_{Sub-B} \\ &= 64\alpha^4 E_{Sub-A}\left\{C_8 \cos\left(8\omega_{R_f} t\right)\right\} \\ &= 32\alpha^4 E_{in}\left[C_{16} + C_{16}\cos\left(16\omega_{R_f} t\right)\right] \end{aligned} \tag{11}$$

From Equation (11), it can be seen that the ±16th order optical sideband signal and the 0th order optical carrier signal are generated in the output signal. In order to obtain the pure ±16th order optical sideband signal, it is necessary to input the output unmodulated optical carrier signal into the OATT, adjust the parameters of the OATT so that the power of the optical signal out of it is the same as the power of the Sub−B's 0th order optical carrier signal, and then adjust the angle of the OPS so that the output of the optical signal and the Sub−B's 0th order optical carrier signal have opposite phases. Finally, after coupling through the power coupler the 0th order optical sideband signal will be cancelled. Its output after coupling can be expressed as

$$\begin{aligned} E_{out} &\approx 32\alpha^4 E_{in}\left\{\left[J_4(m)^4 - 4J_2(m)J_6(m)J_4(m)^2 + 4J_2(m)^2 J_6(m)^2\right]\cos\left(16\omega_{R_f} t\right)\right\} \\ &\approx 32\alpha^4 E_{in}\left[C_{16}\cos\left(16\omega_{R_f} t\right)\right] \end{aligned} \tag{12}$$

Finally, the output optical signal coupled by the coupler is square law detected at the receiving end through the PD, and the electrical signal output from the PD can be expressed as

$$\begin{aligned} I_{PD} &= \zeta G^2 E_{out} \times E^*{}_{out} \\ &\propto \zeta G^2 {E_0}^2\left[{C^2}_{16} + {C^2}_{16}\cos\left(32\omega_{R_f} t\right)\right] \end{aligned} \tag{13}$$

In Equation (13), "G" is the gain factor of the OA, and "ζ" is the responsiveness of the PD to the optical power, and it can be seen that, after reception by the PD, the output signal contains only 32-tupling millimeter wave, which is the millimeter wave signal required by the system.

4. Theoretical Simulation Analysis

According to the main structure depicted in Figure 1, we utilized the optical communication simulation software, Optical System 7.0, to validate the feasibility of our proposed 32-fold millimeter wave generation scheme. Additionally, we analyzed the effects of various non-ideal factors on system stability. The parameter configurations for each component of the simulation system are detailed in Table 1.

Table 1. Parameter configuration of main components in simulation systems.

Device Name	Parameters	Numerical Value
CW laser	Frequency Line width Power	193.1 THz 10 MHz 20 dBm
RF LO	Frequency Amplitude	5 GHz 8.28 v
OPS	Phase shift	180°
OATT	Attenuation coefficient	29.94 dB
OA	Gain	15 dB
MZM	Insertion loss Half-wave voltage Extinction ratio	5 dBm 4.2 V 60 dB
PD	Response Dark current	0.8 A/W 10 nA

Figure 3b shows the spectra of the upper arm and lower arm outputs in Sub-A. It can be seen that when a 90° phase difference exists between the phase of the RF drive signals of the cascaded MZM1 and MZM3, the odd order optical sidebands in the $\pm 2n$d order optical sideband signal are suppressed again. At this time, the output optical sideband signal is a $\pm 4n$ ($n < 4$) order optical sideband, and the output 0th order optical sideband signal component is exactly cancelled out when the modulation coefficient m = 6.12, which is basically consistent with the theoretical analysis in Equation (7). Figure 3c shows the spectrum of Sub-A output. Since there is a 45° phase difference between the RF drive signals loaded onto the upper arm and the lower arm in Sub-A, which causes the $(8n - 4)$-order optical sideband signal output from the lower arm and the $(8n - 4)$-order optical sideband letter output from the upper arm to produce completely opposite phases, the ± 4th order and ± 12th order optically variable band signals are cancelled out during coupling. Only the ± 8th order optical sideband signal is retained in the output optical signal, which is basically consistent with the theoretical analysis in Equation (9). Figure 3d shows the spectrum of the Sub-B output. It can be observed that the output signal generates a new central optical carrier component in addition to the desired ± 16th order optical sideband signal, which is basically consistent with the analysis in Equation (11).

Figure 3a shows the spectrogram of the output of the optical signal in the subsystem Sub-A after passing through a single MZM. When the extinction ratio of the MZM in the system is set to 60 dB and the MZM works at the maximum transmission point, the odd-order optical variable band can be effectively suppressed in the output optical variable band signal, and the output signal contains only the 0th order optical carrier and the $\pm 2n$d order ($n < 6$) optical sideband signals, which is basically consistent with the theoretical analysis.

In order to eliminate the influence of the 0th order optical sideband component on the desired ± 16th order optical sideband signal, the OATT and OPS are used to generate an optical carrier component with the same amplitude and opposite phase as the center optical carrier component all the way to offset the center 0th order optical sideband component generated in the system, and the output is shown in Figure 3e. Figure 3f shows the spectrum of the output after coupling the cancelled optical carriers, and it can be seen that the output retains only ± 16th order optical sideband signals, and the optical variable band rejection ratio of the output through simulation is as high as 52.6 dB.

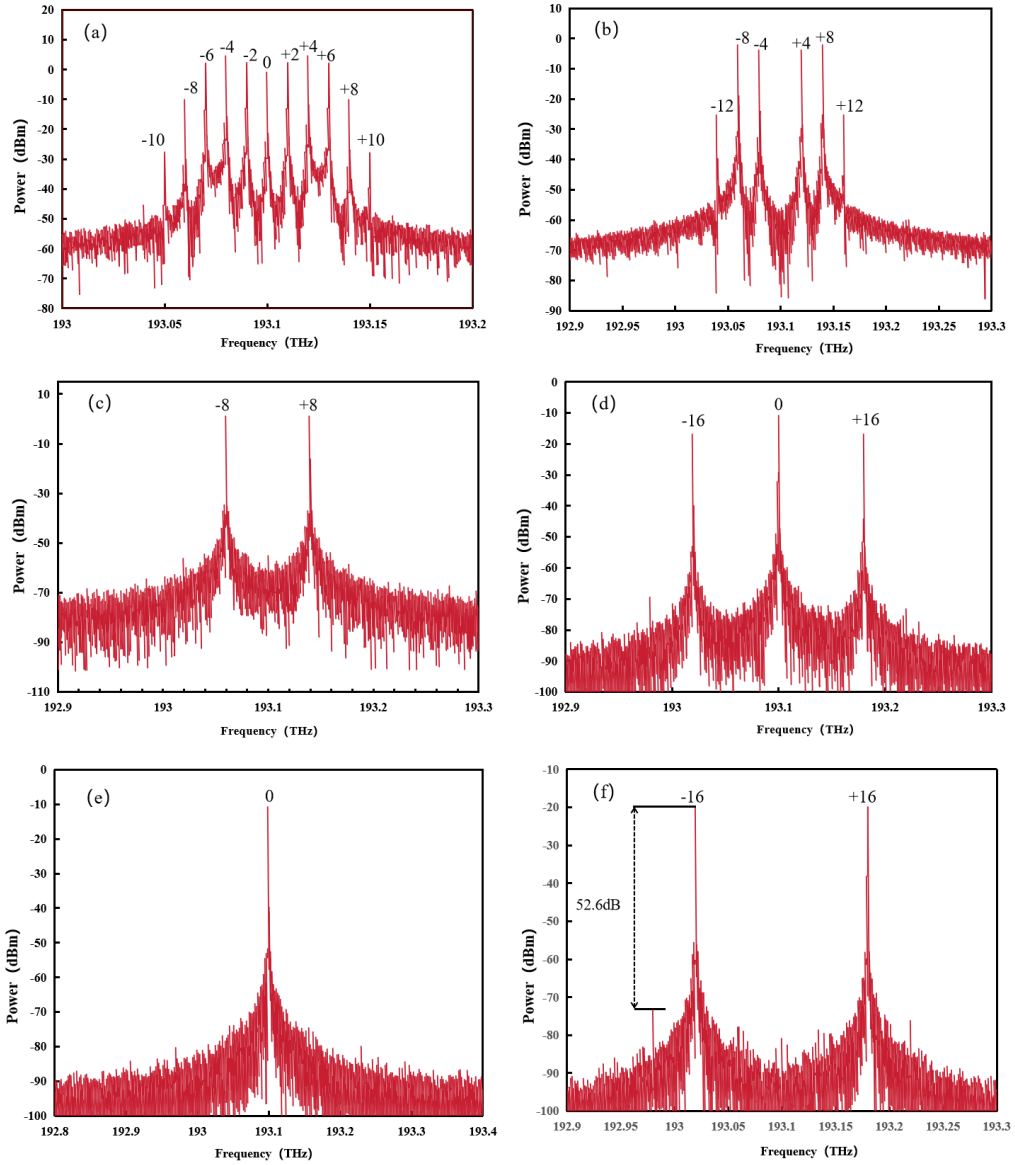

Figure 3. The output spectrum of the system: (**a**) the output spectrum of a single MZM in Sub-A; (**b**) the output spectrum of upper arm and lower arm in Sub-A; (**c**) the output spectrum of Sub-A; (**d**) the output spectrum of Sub-B; (**e**) the spectrum of the output after passing through the OATT and OPS; (**f**) the spectrum of the output after coupling to offset the optical carrier.

Figure 4 shows the spectrum of the electrical signal after PD frequency tapping, and it can be seen from the spectrum that the 160 GHz millimeter wave signal is generated after tapping the level, the spectral purity of the generated frequency doubling signal is high, and the RF sideband rejection ratio of the ultimately obtained millimeter wave signal is as high as 44.75 dB. Compared to the work already presented in [22], the present scheme not only reduces to the modulation index of the system and further improves the multiplication factor of the system, but also ensures that the generated millimeter wave signals have a better performance, and the modulated output signals have a high sideband rejection ratio.

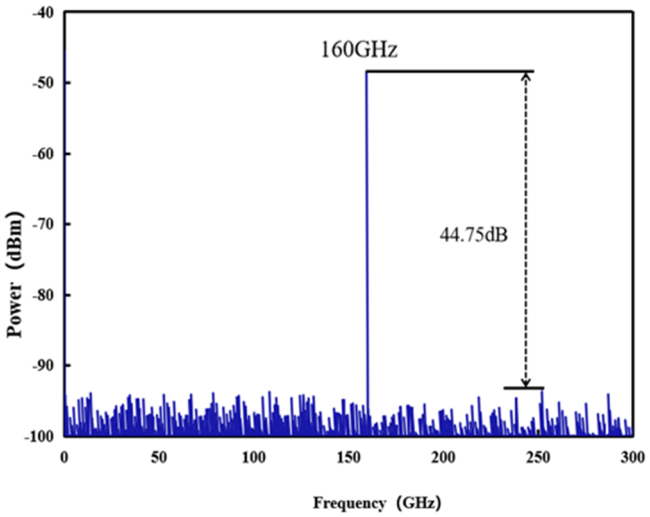

Figure 4. Signal spectrum after a PD beat.

The above analysis process is the structure derived under ideal conditions. In order to explore the impact of non-ideal factors on the performance of the system during practical application, the effects of extinction ratio offset, RF driver phase offset, and modulation index offset on the generated signals OSSR and RFSSR are analyzed respectively in this chapter, and the tolerance ranges of the system for the offsets of each parameter are also given.

In the simulation experiments, we set the parameter of MZM extinction ratio to sweep mode and scanned the effects of different numbers of MZM extinction ratio variations in Sub-A and Sub-B on the generated signal OSSR and RFSSR, respectively, when the extinction ratio is varied from 60 dB to 20 dB, where the number of MZMs in each subsystem is increased from 1 to 4.

Figure 5 shows the effect of extinction ratio variation on the system performance, and it can be seen that when the extinction ratios of all the MZMs in the system are above 55 dB, the variation in OSSR and RFSRR with extinction ratio tends to flatten out, and the effect of extinction ratio on OSSR and RFSRR is not significant. When only the change in MZM extinction ratio in Sub-A is considered, as shown in Figure 5a,c, the OSSR and RFSSR are greater than 18 dB and 29 dB, respectively, when all the MZMs in Sub-A are above 20 dB. When the MZM extinction ratio is greater than 35 dB, the change in RFSSR tends to flatten out with the gradual increase in the MZM extinction ratio, and the RFSSR can reach more than 40 dB. When only the change in MZM extinction ratio in Sub-B is considered, as shown in Figure 5b,d, when all the MZM extinction ratios in Sub-B are more than 20 dB, the OSSR and RFSSR are more than 22 dB and 32 dB, respectively, and when the MZM extinction ratio is more than 35 dB, the change in RFSSR tends to smooth out with the gradual increase in MZM extinction ratio, and RFSSR can reach more than 40 dB. In addition, in practical applications, the signal quality obtained by the system at a commercial MZM with an extinction ratio of 35 dB was verified, taking into account the actual range of variation in commercial MZM extinction ratios [25]. We have inserted the spectrum of the signal obtained under this condition into Figure 5, and it can be seen that the signal obtained under 35 dB extinction ratio still maintains high OSSR and RFSSR, which can meet the requirements of practical engineering applications. However, the millimeter wave production scheme proposed in [29] needs to ensure that the extinction ratio of the MZM in the system needs to be under ideal conditions (extinction ratio tends to infinity) in order to produce high-quality millimeter wave signals, which cannot be achieved in practical applications. The scheme designed in this paper has been simulated and tested, and the Sub-A is able to output high-quality $\pm$8th order optical sideband signals at an extinction ratio of 35 dB, which theoretically can produce high-quality millimeter wave signals using commercial MZMs.

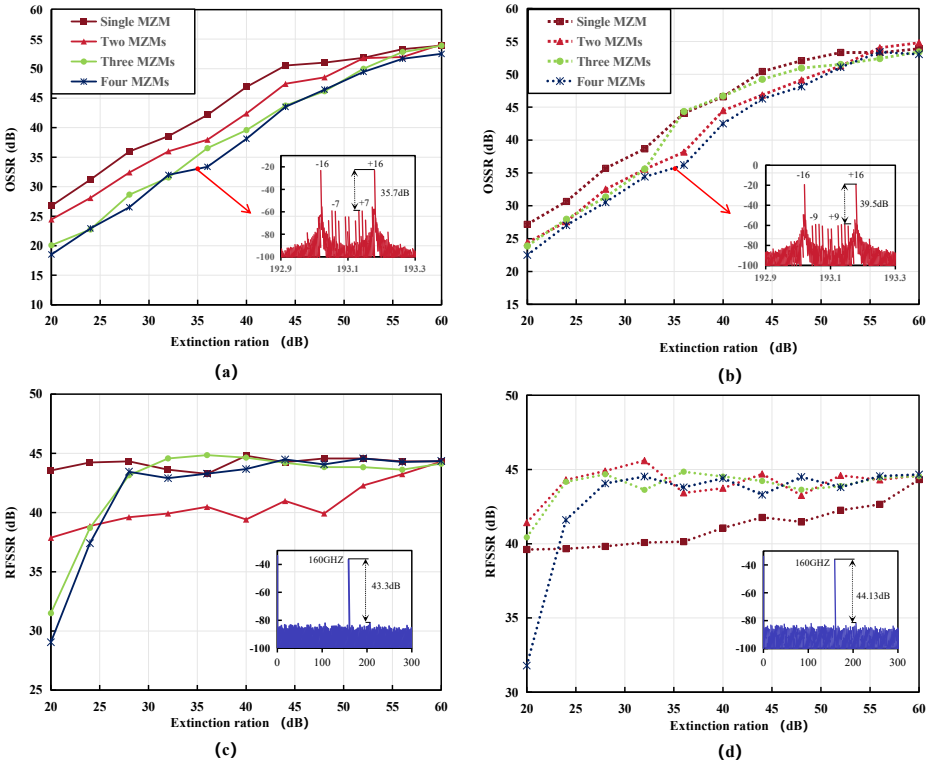

Figure 5. Effects of extinction ratio variation on system performance: (**a**) effects of MZM ER variation on OSSR in Sub-A; (**b**) effects of MZM ER variation on OSSR in Sub-B; (**c**) effects of MZM ER variation on RFSSR in Sub-A; (**d**) the effect of MZM ER on RFSSR in Sub-B.

Figure 6 shows the effect of RF drive signal phase shift on OSSR and RFSSR. During the experimental analysis, the phase shift analysis was carried out for the EPS initial phase of 45°, 90°, and 135°, respectively, and the sweep reference was carried out for the deviation initial term phase value of ±2°. It was found that when the initial phase of the EPS of 45°, 90°, and 135° was shifted within the range of ±2°, the effects on the generated OSSR and RFSSR of the signals are in accordance with the variation curves in Figure 6. It can be seen that when the initial phase shift is in the range of ±1°, the quality of the generated millimeter wave signals decreases rapidly, with the OSSR decreasing from 54 dB to 23 dB and the RFSSR decreasing from 44.5 dB to 16.05 dB. This is due to the fact that the output signals are unable to eliminate the spurious optical variable band signals of different orders when the phase of the EPS is shifted away from the ideal value. When the initial phase shift is larger than ±1°, the changes of OSSR and RFSSR gradually level off with the increase in the offset, and the OSSR and RFSSR gradually decrease to less than 20 dB and 15 dB, respectively. Therefore, in order to ensure the performance of millimeter wave signals generated in the process of practical application, the ideal value of the phase shift of the EPS should be controlled to be within the range of ±1° as far as possible.

Figure 7 shows the effect of modulation index offset on the OSSR and RFSSR of the generated signal. It can be seen that when the modulation index is not offset, that is, m = 6.12, the OSSR and RFSSR of the generated signal reach their extreme values. When the modulation index offset is within the ideal range of 0.4%, due to nonlinear effects, the power of the central optical carrier component and ±8th order optical sideband component gradually increases. OSSSR decreases from 54 dB to 19.4 dB, and RFSSR decreases from 45 dB to 12.9 dB. When the offset ideal value exceeds 0.4%, the decrease in OSSR and RFSSR tends to stabilize with the increase in modulation index offset, but due to the gradual increase in ±8th order optical sideband component, the decrease in OSSR and RFSSR tends to stabilize. The generated millimeter wave signal cannot meet the actual reference requirements. Compared to the schemes proposed in [30,31], the

millimeter wave generation scheme proposed in this paper has a lower modulation index requirement of 2.44 and 2.22, respectively, further reducing the system's requirements for modulation index.

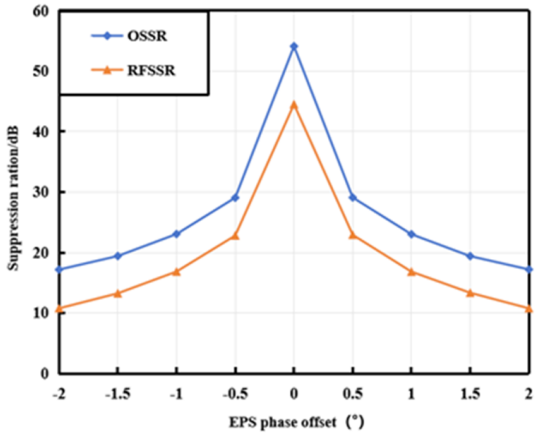

Figure 6. The effect of RF drive signal phase shift on OSSR and RFSSR.

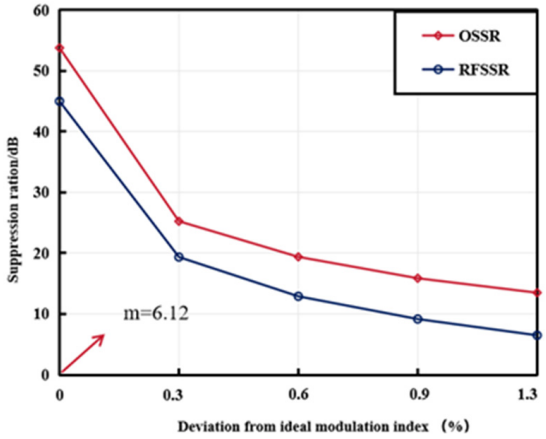

Figure 7. The impact of modulation index offset on OSSR and RFSSR.

Figure 8 shows the spectrum and RF spectrum when the modulation index m = 6.2. At this time, the modulation index is shifted by more than 1.3% relative to the ideal value. It can be seen that in the output spectrum, in addition to the required ±16th order optical sidebands, there is also the spurious central optical carrier component and the ±8th order optical sideband signals, which is basically the same as the above analysis. The ±8th order spurious optical sideband component becomes a main factor affecting the signal quality and the generated millimeter wave. The OSSR of the generated millimeter-wave signal decreases to 13.5 dB, and the output RF spectrum contains the spurious signal components of 40 GHz, 80 GHz, and 120 GHz, in addition to the required 160 GHz millimeter wave component, and the RFSSR is only 7.5 dB. Therefore, in order to ensure that the quality of the generated millimeter wave signals meets the requirements of the system transmission, the offset range of the modulation index of the system should be 0.4% or less.

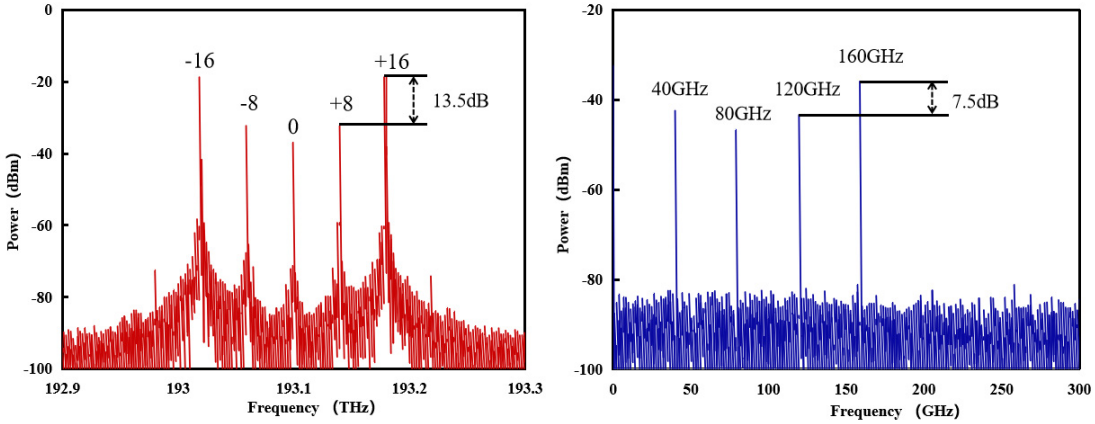

Figure 8. Spectral and RF spectra at modulation index m = 6.2.

5. Conclusions

In this paper, a new method based on the cascade of eight MZMs to generate a 32-tupling millimeter wave signal using a 5 GHz signal to generate a 160 GHz millimeter wave signal is proposed, and the system structural principle is described in detail and verified by theoretical analysis and simulation, which does not require the introduction of any optical filtering elements in this scheme. By adjusting the parameters of modulation index m, EPS, OA, OATT, and OPS of the MZM, the irrelevant spurious harmonics can be suppressed so that the optical signal only outputs ±8th order sidebands after Sub-A, and only outputs ±16th order sidebands after Sub-B, and finally achieves the signal's 32-tupling frequency multiplication by the PD reception beat, and its OSSR and RFSSR are 52.6 dB and 44.75 dB. The effects of device parameter variations on the system under non-ideal conditions are also analyzed and the tolerable range of the system is given. Compared with the proposed 32-tupling-frequency millimeter wave generation scheme, the present scheme can still generate high-quality millimeter wave signals under the conditions of modulation index m = 6.12 and extinction ratio less than 35 dB, which reduces the system requirements for MZM modulation index and extinction ratio and greatly improves the tunable performance of the system.

Author Contributions: Conceptualization, L.R. and X.W.; methodology, X.Y.; software, X.Y. and D.W.; validation, D.W. and L.R.; formal analysis, X.Y. and D.W.; data curation, X.Y.; writing—original draft preparation, L.R.; writing—review and editing, L.R. and X.W.; visualization, D.W.; supervision, X.Y.; funding acquisition, X.W. All authors have read and agreed to the published version of the manuscript.

Funding: This research work was supported in part by Scientific Research Project of Fuyang Normal University (2022KYQD0004) and Anhui Education Department, and University Natural Science Research Project of Anhui Province (Grant No.: 2022AH051338). This work was supported by Henan Key Laboratory of Visible Light Communications (No. HKLVLC2023-B10), Jiangxi Provincial Natural Science Foundation (20232BAB212006) and Open Fund of Advanced Cryptography and System Security Key Laboratory of Sichuan Province (Grant No. SKLACSS-202306) and (Grant No. SKLACSS-202303). Anhui Digital Intelligent Engineering Research Center for Agricultural Products Quality Safety (APDI202302).

Data Availability Statement: The simulated and experimental data that support this work are available from the corresponding author upon reasonable request.

Conflicts of Interest: The authors declare that they have no known competing financial interests or personal relationships that could have appeared to influence the work reported in this paper.

References

1. Anes, B.; Riad, B.A. Filterless Photonic Millimeter Wave Generation and Data Transmission for 5G Indoor Wireless Access. *Microw. Rev.* **2022**, *28*, 30–39.
2. Ehsan, E.; Ngah, R.; Daud, N.A.B. A 1.792 Tbps RoF-based PDM-DQPSK DWDM system for high-capacity long-haul 5G and beyond optical network. *Optik* **2022**, *269*, 169858. [CrossRef]
3. Akyildiz, I.F.; Han, C.; Nie, S. Combating the distance problem in the millimeter wave and terahertz frequency bands. *IEEE Commun. Mag.* **2018**, *56*, 102–108. [CrossRef]
4. Bauer, M.; Friederich, F. Terahertz and millimeter wave sensing and applications. *Sensors* **2022**, *22*, 9693. [CrossRef]
5. Li, X.; Yu, J. W-band RoF transmission based on optical multi-carrier generation by cascading one directly-modulated DFB laser and one phase modulator. *Opt. Commun.* **2015**, *345*, 80–85. [CrossRef]
6. Zhou, Y.; Dong, Y.; Hou, F.; Wu, J. Review on Millimeter-Wave Radar and Camera Fusion Technology. *Sustainability* **2022**, *14*, 5114. [CrossRef]
7. Novak, D.; Waterhouse, R.B.; Nirmalathas, A.; Lim, C.; Gamage, P.A.; Clark, T.R.; Dennis, M.L.; Nanzer, J.A. Radio-over-fiber technologies for emerging wireless systems. *IEEE J. Quantum Electron.* **2015**, *52*, 1–11. [CrossRef]
8. Chen, S.; Zhao, J. The requirements, challenges, and technologies for 5G of terrestrial mobile telecommunication. *IEEE Commun. Mag.* **2014**, *52*, 36–43. [CrossRef]
9. Han, Y.-S.; Zheng, Z.; Luo, Z.; Min, Z.; Xu, O.; Liu, J. High-power optical millimeter-wave signal generation with tunable frequency multiplication factor. *Opt. Commun.* **2015**, *335*, 53–59. [CrossRef]
10. Pi, Z.; Khan, F. An introduction to millimeter-wave mobile broadband systems. *IEEE Commun. Mag.* **2011**, *49*, 101–107. [CrossRef]
11. Yu, J. Photonics-assisted millimeter-wave wireless communication. *IEEE J. Quantum Electron.* **2017**, *53*, 1–17. [CrossRef]
12. Ramos, R.; Seeds, A. Fast heterodyne optical phase-lock loop using double quantum well laser diodes. *Electron. Lett.* **1992**, *1*, 82–83. [CrossRef]
13. Yu, Y.; Dong, J.; Li, X.; Zhang, X. Photonic generation of millimeter-wave ultra-wideband signal using phase modulation to intensity modulation conversion and frequency up-conversion. *Opt. Commun.* **2012**, *285*, 1748–1752. [CrossRef]
14. Zheng, H.; Liu, S.; Li, X.; Wang, W.; Tian, Z. Generation and transmission simulation of 60 G millimeter-wave by using semiconductor optical amplifiers for radio-over-fiber systems. *Opt. Commun.* **2009**, *282*, 4440–4444. [CrossRef]
15. Shih, P.T.; Chen, J.; Lin, C.T.; Jiang, W.J.; Huang, H.S.; Peng, P.C.; Chi, S. Optical millimeter-wave signal generation via frequency 12-tupling. *J. Light. Technol.* **2009**, *28*, 71–78. [CrossRef]
16. Al-Dabbagh, R.; Al-Raweshidy, H. Photonic methods of millimeter-wave generation based on Brillouin fiber laser. *Opt. Laser Technol.* **2016**, *79*, 124–131. [CrossRef]
17. Park, C.S.; Lee, C.G.; Park, C.S. Photonic frequency upconversion by SBS-based frequency tripling. *J. Light. Technol.* **2007**, *25*, 1711–1718. [CrossRef]
18. Chen, L.; Pi, Y.; Wen, H.; Wen, S. All-optical mm-wave generation by using direct-modulation DFB laser and external modulator. *Microw. Opt. Technol. Lett.* **2007**, *49*, 1265–1267. [CrossRef]
19. Wu, P.; Ma, J. BPSK optical mm-wave signal generation by septupling frequency via a single optical phase modulator. *Opt. Commun.* **2016**, *374*, 69–74. [CrossRef]
20. Li, X.; Xiao, J.; Xu, Y.; Chen, L.; Yu, J. Frequency-doubling photonic vector millimeter-wave signal generation from one DML. *IEEE Photonics J.* **2015**, *7*, 1–7. [CrossRef]
21. Zhu, Z.; Zhao, S.; Li, Y.; Chen, X.; Li, X. A novel scheme for high-quality 120 GHz optical millimeter-wave generation without optical filter. *Opt. Laser Technol.* **2015**, *65*, 29–35. [CrossRef]
22. Wang, D.; Tang, X.; Xi, L.; Zhang, X.; Fan, Y. A filterless scheme of generating frequency 16-tupling millimeter-wave based on only two MZMs. *Opt. Laser Technol.* **2019**, *116*, 7–12. [CrossRef]
23. Chen, X.; Liu, X.; Dai, S.; Li, Z.; Ba, W.; Wang, D. Generation of frequency 32-tupling millimeter-wave based on a dual-parallel polarization modulator. *Appl. Opt.* **2021**, *61*, 294–301. [CrossRef] [PubMed]
24. Shanmugapriya, G. Frequency16-tupled optical millimeter wave generation using dual cascaded MZMs and 2.5 Gbps RoF transmission. *Optik* **2017**, *140*, 338–346.
25. Chen, X.; Dai, S.; Li, Z.; Ba, W.; Chen, X. Thirty-two-tupling frequency millimeter-wave generation based on eight Mach–Zehnder modulators connected in parallel. *ETRI J.* **2023**, *46*, 194–204. [CrossRef]
26. Liu, J.; Zhou, G.; Du, J.; Shen, W.; Zhou, L.; He, Z. Silicon mode-loop Mach-Zehnder modulator with L-shaped PN junction for 0.37 V· cm V π L high-efficiency modulation. *Photonics Res.* **2021**, *10*, 214–221. [CrossRef]
27. Dar, A.B.; Ahmad, F.; Jha, R.K. Filterless optical millimeter-wave generation using cascaded-parallel Mach–Zehnder modulators with tunable frequency multiplication factor. *Opt. Quantum Electron.* **2021**, *53*, 1–15. [CrossRef]
28. Mohamed, M.; Zhang, X.; Hraimel, B.; Wu, K. Efficient Photonic Generation of Millimeter-Waves Using Optical Frequency Multiplication in Radio-over-fiber Systems. In Proceedings of the IEEE International Topical Meeting on Microwave Photonics. IEEE, Victoria, BC, Canada, 2–5 October 2007.
29. Baskaran, M.; Prabakaran, R. Optical millimeter wave signal generation with frequency 16-tupling using cascaded mzms and no optical filtering for radio over fiber system. *J. Eur. Opt. Soc. Rapid Publ.* **2018**, *14*, 13. [CrossRef]

30. Chen, X.Q.; Liu, X.R.; Li, Z.H. A filterless frequency 32-tupling photonic scheme to generate Sub-Terahertz wave signal enabled by optical polarization modulators. *Opt. Quantum Electron.* **2021**, *53*, 663. [CrossRef]
31. Chen, X.; Dai, S.; Li, Z.; Liu, X.; Chen, X.; Xiao, H. Filterless frequency 32-tupling millimeter-wave generation based on two cascaded dual-parallel Mach–Zehnder modulators. *Front. Phys.* **2023**, *11*, 1212482. [CrossRef]